THE JOURNAL OF PHYSICAL CHEMISTRY B

ARTICLE

pubs.acs.org/JPCB

Structural Stability from Solution to the Gas Phase: Native Solution Structure of Ubiquitin Survives Analysis in a Solvent-Free Ion Mobility−Mass Spectrometry Environment

Thomas Wyttenbach and Michael T. Bowers*

Department of Chemistry and Biochemistry, University of California Santa Barbara, Santa Barbara, California 93106, United States

Supporting Information

ABSTRACT: The conformations of desolvated ubiquitin ions, lifted into the gas phase by electrospray ionization (ESI), were characterized by ion mobility spectrometry (IMS) and compared to the solution structures they originated from. The IMS instrument combining a two-meter helium drift tube with a quadrupole time-of-flight mass spectrometer was built in-house. Solutions stabilizing the native state of ubiquitin yielded essentially one family of tightly folded desolvated ubiquitin structures with a cross section matching the size of the native state (1000 Å^2). Solutions favoring the *A* state yielded several well-defined families of significantly unfolded conformations (1800−2000 Å^2) matching in size conformations between the *A* state and a fully unfolded state. On the basis of these results and a wealth of data available in the literature, we conclude that the native state of ubiquitin is preserved in the transition from solution to the desolvated state during the ESI process and survives for >100 ms in a 294 K solvent-free environment. The *A* state, however, is charged more extensively than the native state during ESI and decays more rapidly following ESI. *A* state ions unfold on a time scale equal to or shorter than the experiment (≤50 ms) to more extended structures.

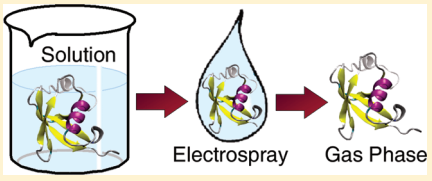

INTRODUCTION

Over the course of the last two decades, mass spectrometry (MS) has evolved into one of the most powerful analytical tools available in biochemistry. Some of the most notable advantages of MS include sensitivity, speed, small sample consumption, and the ability to deal with complex mixtures. In a system of rapid equilibria of interconverting species, such as in a solution of rapidly aggregating protein, MS is virtually the only method allowing isolation and characterization of one particular component in the mixture, for instance the trimer in the aggregating protein solution.[1] Bulk analysis methods (CD, NMR, etc.) applied to a complex mixture are often not able to reveal any information about one particular species of interest present in the mixture for a number of reasons: bulk data may be saturated by high-abundance components fully obscuring a low-abundance species of interest; the data may be characteristic of the average of all components rather than the component of interest; the data may be too complex to be interpreted.

Because of the advantages MS has to offer, it is of great interest to develop MS-based methods to characterize the analyte not only by mass but also by other properties. Molecular structure is a property of particular interest to chemists and biochemists. Whereas presently available MS−MS methods applied to biopolymers provide structural sequence information (primary structure), it is highly desirable to develop additional MS-based methods elucidating the three-dimensional molecular structure (secondary/tertiary structure of biopolymers). MS coupled to spectroscopy, ion mobility spectrometry (IMS), or methods probing the conformation-dependent chemical reactivity such as H/D exchange, HI attachment, electron capture dissociation (ECD), blackbody infrared radiative dissociation (BIRD), and other methods have the potential of probing molecular structure in detail while benefiting from the advantages of MS.[2−8]

In our laboratories, we have developed instrumentation combining MS with IMS designed to probe the three-dimensional structure of molecules. IMS data provide information about the overall shape of a molecule and yield, together with supplemental theoretical studies such as electronic structure calculations and molecular dynamics (MD) simulations, detailed information about the three-dimensional arrangement of atoms within the molecule.[3] However, an important question has to be addressed: Is the structural information of a molecule probed in the vacuum of a mass spectrometer relevant in the context of the chemistry of interest? For instance, whereas the mass spectrometer environment may be adequate for research of interstellar space, the complete absence of solvent in the mass spectrometer may be of great concern for a researcher interested in solution chemistry. Questions regarding the effect of solvent on the analyte structure detected in the IMS−MS experiment have to be addressed.

Electrospray ionization[9] (ESI) is one of many methods to introduce the analyte into the mass spectrometer. Whereas most traditional ionization sources employed in MS require the analyte to be present as a gas, ESI methods do not depend on the presence of a substantial analyte vapor pressure. Therefore, ESI can readily be applied to macromolecular analytes in the kilodalton to

Received: July 18, 2011
Revised: August 31, 2011
Published: September 09, 2011

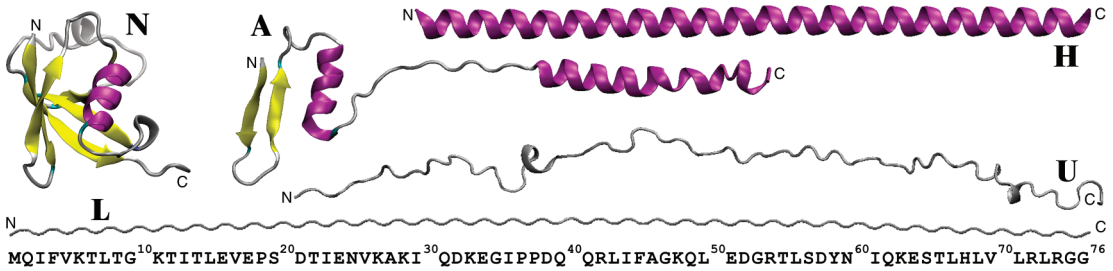

Figure 1. Various conformations and the human sequence of the 76 residue protein ubiquitin. **N** is the native state characterized by X-ray crystallography and NMR; **A** the *A* state found in acidic solutions containing high concentrations of methanol; **H** a hypothetical fully α-helical conformation (all backbone dihedral angles set to $\phi = -57°$ and $\psi = -47°$); **U** an unfolded conformation found in MD simulations of $[M + 13H]^{+13}$ in a solvent-free environment;[52] and **L** a hypothetical fully linear conformation ($\phi = \psi = 180°$). All structures are rotated such that their N terminus is on the left and their C terminus is on the right with the termini labeled by nonbold letters N and C, respectively.

megadalton range and beyond.[10,11] In addition, ESI is a "soft" ionization method lifting the analyte gently into the gas phase as intact molecules. However, of particular interest in the context of structural analysis is the fact that ESI provides an opportunity to couple an analyte *solution* directly to the mass spectrometer. Hence, in ESI, analyte molecules are rapidly desolvated as the solution is sprayed through the small (1−10 μm) orifice of a capillary in the presence of an electric field (~1 kV/mm). Whereas understanding the exact mechanism of solvent evaporation in ESI is still an active field of research, it is established that the electric field produces a very fine spray of tiny charged droplets.[12−17] The large surface area of the system promotes rapid solvent evaporation yielding quickly a gas mixture of neutral and charged solvent and analyte particles. Neutral particles are pumped away in the source region and/or get lost due to random diffusion, whereas ionic particles are collected and focused into the mass spectrometer employing DC and/or RF electric fields. Ions which are expected to be subthermal due to evaporative cooling are ready for analysis within microseconds to milliseconds after desolvation depending on the experimental setup. The charge present on analyte *cations* is typically the result of excess protons (organic analyte) and/or alkali ions (any analyte), whereas opposite polarity in the electric fields yields a collection of proton-deficient analyte *anions*.

In general, there will be differences between solution and solvent-free structures which can be substantial. The question, then, is how long does the transformation from solution structure to solvent-free structure take once the solvent has evaporated?[18] Experiments on a range of proteins and oligonucleotides indicate that ESI-generated ions often retain significant aspects of their solution structure.[11,19−34] Solution structure retention can readily be demonstrated in an annealing experiment carried out following ESI. An example from our laboratories includes the calcium-binding protein calmodulin.[27] When calmodulin ions (charge state 8) emerge directly from the ESI source and are sampled under gentle operating conditions, they are found to be compact. However, under experimental conditions favoring annealing into gas-phase structures, significantly more extended structures are observed.[27] This experiment shows unambiguously that in the absence of high-energy collisions the structures of the ESI-generated protein ions do not resemble equilibrated gas-phase structures at all. Since they originate from solution, these metastable protein ions are likely to resemble solution structures more closely than gas-phase structures.

In another example from our laboratory, the amyloid β-protein (Aβ) implicated in Alzheimer's disease, high-level MD simulations indicate that the hydrophilic side chains of this 4.5 kDa peptide interact with the solvent water, whereas the hydrophobic residues tend to be buried in the interior of the structure.[35] However, simulated Aβ structures equilibrated in the absence of solvent show the opposite trend: hydrophilic residues interact with each other in the center of the structure, and hydrophobic residues decorate the surface. Hence, interconversion from a solution equilibrium structure to an equilibrated solvent-free geometry often involves very large structural rearrangements with potentially high barriers. Macromolecular motions involving the entire molecule are known to occur on a time scale of up to seconds for proteins in solution, and in the absence of solvent they may take even longer. Breaking an intramolecular interaction during a conformational transition is energetically less favorable in vacuum than in solution where the loss of such an interaction can be partially compensated by formation of an intermolecular interaction with the solvent. This leads to transition states which are higher in energy in the absence of solvent and slower kinetics. Gas-phase equilibration may take up to minutes and hours.[36]

In this study, we focus on the nature of the structures that emerge from an ESI source and how closely these structures resemble solution geometries. We chose ubiquitin as a target protein because it is small in size and is well characterized. The human form of ubiquitin (which is identical for virtually all animal species) is composed of 76 residues with the sequence shown in Figure 1. The function of ubiquitin is to tag target proteins via covalent attachment (ubiquitination), most prominently for proteasomal degradation. The native state of ubiquitin has been characterized by X-ray crystallography and NMR and is tightly folded containing both α-helix and β-sheet secondary structure elements (Figure 1).[37−40] This structure is very stable in aqueous solution and resists denaturing even upon addition of significant amounts of organic solvents. The native state is also stable over a large pH range in aqueous solution. However, in acidic solutions with high concentrations of methanol, ubiquitin rearranges to a less compact partially folded form, the *A* state (Figure 1).[41−43] As a consequence, we will have a good idea of its structure in solution before we spray it and analyze it using IMS−MS.

Not only is ubiquitin well characterized in the crystal and in solution but also the literature includes a number of gas-phase studies, some IMS-based. Hence, the purpose of choosing ubiquitin is not to venture into uncharted IMS territory. In this work, a wealth of available ubiquitin data is an advantage. We strive to understand the data, ours and that in the literature, in the context of the structural evolution in the ESI desolvation process. Gas-phase studies include the pioneering IMS work by Clemmer

and co-workers,[31−34] electron capture dissociation (ECD) studies by Breuker and McLafferty and co-workers,[7,44] a number of studies based on H/D-exchange[36,45,46] or field asymmetric waveform IMS (FAIMS),[46−50] and recent work by Julian and co-workers employing radical-directed dissociation (RDD) methods.[51] Aspects of some of this work will be commented on once we present the results of the current study.

METHODS

A ubiquitin stock solution was prepared by dissolution in HPLC-grade pure water (J.T. Baker, Phillipsburg, NJ) of bovine erythrocytes ubiquitin (≥90% purity) purchased from Sigma (St. Louis, MO) and used without further purification. ESI spray solutions contained a small aliquot of stock solution diluted to 8 μM ubiquitin concentration in one of the appropriate solvents or solvent mixtures. Four ESI solution conditions were used: (1) pure water, (2) 1% acetic acid (EM Science, Gibbstown, NJ) in water, (3) a 1:1 mixture of water and methanol (Fisher Scientific, Fair Lawn, NJ), and (4) 1% acetic acid in a 1:1 mixture of water and methanol. For IMS−MS analysis, ∼10 μL of spray solution is used to fill an ESI nanospray tip supplying an ion signal for up to several hours. Spray tips are made of a borosilicate glass tube (1.2 mm o.d., 0.69 mm i.d.; Sutter Instrument, Novato, CA) pulled on one side into a fine filament on a Sutter Instrument (Novato, CA) micropipet puller and gold coated on an Emitech (Kent, U.K.) sputter coater.[53]

Nano-ESI takes place in air at atmospheric pressure and room temperature. A stainless steel capillary (75 mm long × 0.25 mm i.d.) held at room temperature serves as the interface to the vacuum of the IMS−MS instrument. The spray voltage applied to the spray tip with respect to the stainless steel capillary across a ∼3 mm gap is kept as low as possible, typically at 800−1000 V.

The IMS−MS instrument was built in house and has previously been described in detail.[54] Briefly, ESI-generated ions exiting the source capillary enter an hourglass ion funnel located in the source vacuum chamber which is connected to a pump and held at a constant pressure of 0.18 Torr below the drift tube pressure. The ion funnel guides the ions toward the IMS drift tube entrance where they are accumulated and then pulsed into the drift tube with a frequency of 5−20 Hz. The drift tube is held at room temperature (294 K) and is filled with 10−15 Torr of helium gas. The drift field across the 2 m length of the tube is 1−4 kV, yielding ubiquitin ion drift times of 50−200 ms. Ions exiting the drift region are refocused in a second ion funnel which leads to a small orifice, the interface to the high vacuum of the mass spectrometer. Following the drift tube, ions are mass analyzed using a quadrupole mass filter. To obtain ion mobility spectra of mass-selected ions, the quadrupole is set to transmit a given mass-to-charge ratio (m/z), and the ion arrival time distribution (ATD) is recorded at the detector. To obtain mass spectra, ion pulsing prior to ion mobility dispersion is omitted, and the quadrupole mass filter is scanned.

The connection between drift time measured in the ATD and the absolute cross section is rigorously given by kinetic theory.[3,55] Experimental cross sections are reproducible to <0.5%, and systematic errors of absolute cross sections are expected to be of the order of 1%. The instrument resolution for multiply charged ions is 100−150, and it is given predominantly by the initial pulse width and the spread of the ion cloud in the RF field of the ion funnel following the drift tube.

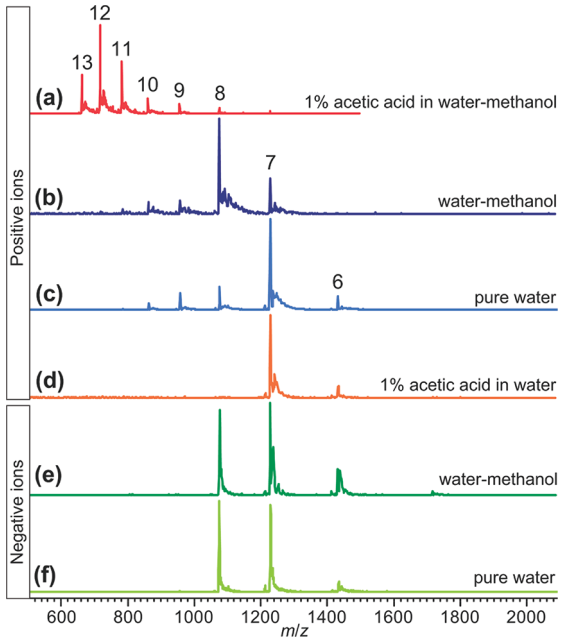

Figure 2. Positive and negative ion mass spectra of ubiquitin as a function of ESI solution condition. (a) Positive ion spectrum obtained under typical ESI conditions employing a solvent of 1% acetic acid in 1:1 water−methanol. In this solvent mixture ubiquitin is known to occur in the *A* state. The native state, on the other hand, is known to be stable under all other solvent conditions used here: In positive ion mode, (b) 1:1 water−methanol, (c) pure water, (d) 1% acetic acid in water; and in negative ion mode, (e) 1:1 water−methanol and (f) pure water. The numbers above the peaks indicate the charge state of ubiquitin.

Since collision cross sections measured for ubiquitin ions directly reflect the folding of the protein, it is interesting to compare the experimental data with the cross section values theoretically expected for a ubiquitin molecule in various structural states (see Figure 1). We employ an "exact hard sphere scattering" (EHSS) model to evaluate the scattering processes occurring between helium and the model molecule structure.[56] The accuracy of theoretical EHSS cross sections is limited, and agreement with experiment within several percent has to be considered a possible match.

RESULTS

Figure 2 shows ubiquitin ESI mass spectra taken under various solution conditions, as labeled in the figure. In panel a (1% acetic acid in 1:1 water−methanol), the major peaks correspond to ubiquitin with an excess of 11, 12, and 13 protons, $[M + zH]^{+z}$ ($z = 11-13$). Ubiquitin contains one histidine, seven lysine, four arginine residues, and an N-terminal amino group and can therefore readily accommodate up to 13 protons.

Panel b gives a spectrum employing a pH-neutral solution (1:1 water−methanol, no acid) with intense peaks for $[M + 7H]^{+7}$ and $[M + 8H]^{+8}$. Charge states 11, 12, and 13 are essentially absent. Similar spectra are obtained in pure water and, interestingly, in an acidic aqueous solution (1% acetic acid in water) (panels c and d).

Negative ion ESI mass spectra are shown in panels e and f for a 1:1 water−methanol mixture and in pure water, respectively. In both cases, 7- and 8-fold deprotonated ions $[M - zH]^{-z}$ are most abundant. Ubiquitin contains 12 carboxylic acid functional

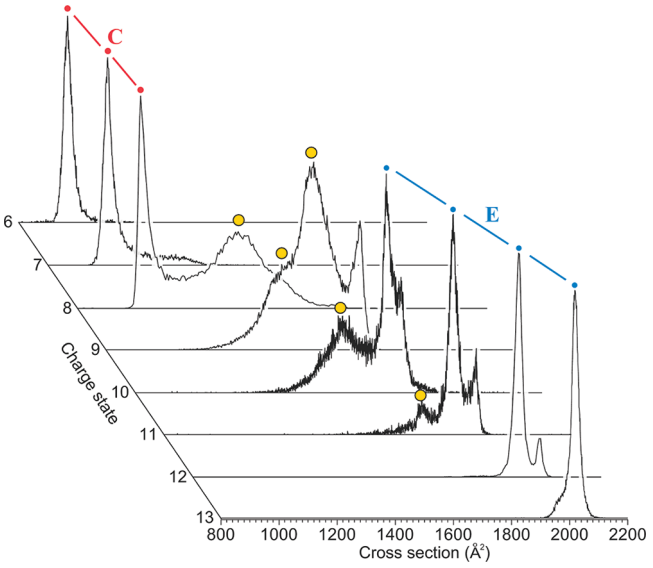

Figure 3. Ion mobility spectra of mass-selected positive ubiquitin ions as a function of charge state. Drift times (x-axis) are normalized by ion charge, helium pressure, and drift voltage in each case and are therefore proportional to cross sections indicated in units of Å^2. This representation allows direct comparison of features across spectra. Ion drift times are of the order of 40−100 ms in all spectra. Apparent are several sharp peaks (marked in red) corresponding to a family **C** of ions with a cross section of ∼1000 Å^2 and a charge of 6−8. Another set of sharp intense peaks **E** (blue) occurs in the range of 1600−2000 Å^2 for charge states 10 and above. Broad features observed for ions of intermediate charge and intermediate cross section are marked with a large yellow dot. Solvents used for acquisition of the spectra are pure water for z = 6 and 7; 1:1 water−methanol for z = 8 and 9; and 1% acetic acid in 1:1 water−methanol for z = 10−13.

groups (including the C terminus) allowing this protein to be multiply anionic by loss of protons. Acidic ubiquitin solutions did not yield any signal in the negative ion mode.

Ion mobility spectra obtained for various m/z-selected ubiquitin ions $[M \pm zH]^{\pm z}$ are shown in Figures 3 and 4 as a function of charge state z and of spray solution condition, respectively. The major features in the ATDs peak around 40−100 ms in all spectra shown. However, since drift times are normalized by the helium pressure, drift voltage, and ion charge z in the presentation chosen in Figures 3 and 4, the drift time is directly proportional to the collision cross section[3,55] and is therefore shown in units of Å^2. Whereas the lower charge state ions, z = ±6, ±7, and ±8, show a sharp peak around 1000 Å^2 (Figure 3), more extensively charged ubiquitin, z = 10−13, forms one or two sharp peaks in the 1700−2000 Å^2 range. In addition, the spectra of the intermediate charge states z = 8−11 display broad peaks of several unresolved species in the 1300−1700 Å^2 range. These general trends as a function of charge state hold for all solution conditions employed here.

Figure 4 examines the effect of spray solution in more detail. Most typically, ion mobility spectra of a given charge state do not depend significantly on the choice of solvent or pH for the four solution conditions considered here (pure water; 1:1 water−methanol; 1% acetic acid in water; 1% acetic acid in 1:1 water−methanol). This is demonstrated in Figure 4a−c and f for the examples of charge states ±6, ±7, −8, and +11. In particular, the positions of the sharp peaks are reproduced from one solvent to the other within <0.5%. If more than one peak is present in the spectrum, subtle differences may occur in the relative intensity of

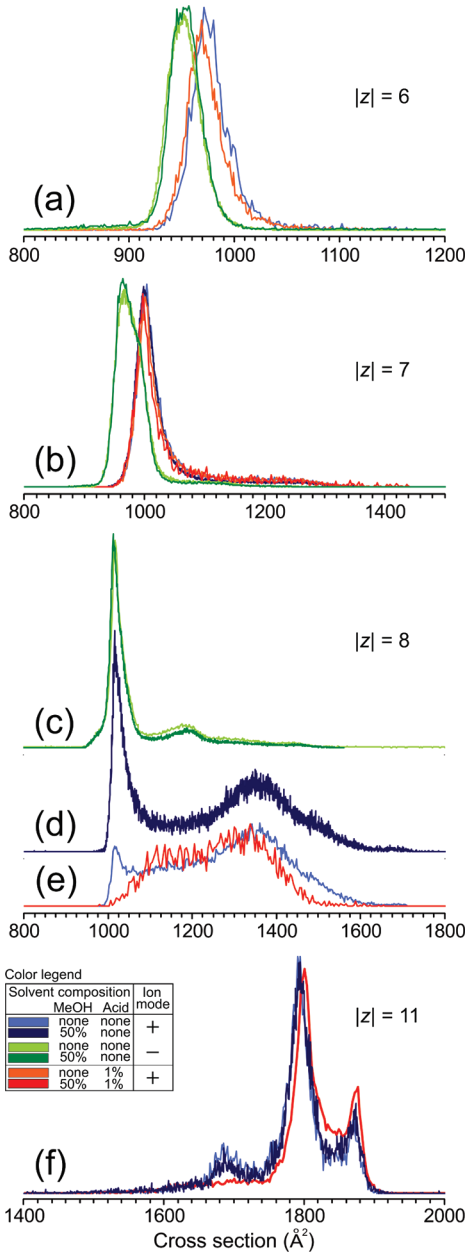

Figure 4. Ion mobility spectra of mass-selected ubiquitin ions as a function of ion mode (positive or negative) and ESI solvent composition for a selection of charge states: (a) ±6, (b) ±7, (c) −8, (d) and (e) +8, and (f) +11. Shown in blue are spectra for positive ions sprayed from pure water (light blue) or from a 1:1 water−methanol mixture (dark blue). Shown in green are spectra for negative ions sprayed from pure water (light green) or from a 1:1 water−methanol mixture (dark green). Shown in orange and red are spectra for positive ions sprayed from 1% acetic acid in water (orange) or 1% acidic acid in 1:1 water−methanol (red).

peaks. For instance, the peak at 1690 Å^2 in the z = 11 spectrum (Figure 4f) is more pronounced in the absence of acetic acid. However, charge state +8 is an exception. In the z = 8 data shown in Figure 4d and e, the relative intensity of the sharp peak at 1000 Å^2 varies strongly relative to the broad feature around 1350 Å^2 as solution conditions vary.

A comparison of positive and negative ion mobility data shows significant similarities for $[M + zH]^{+z}$ and $[M - zH]^{-z}$

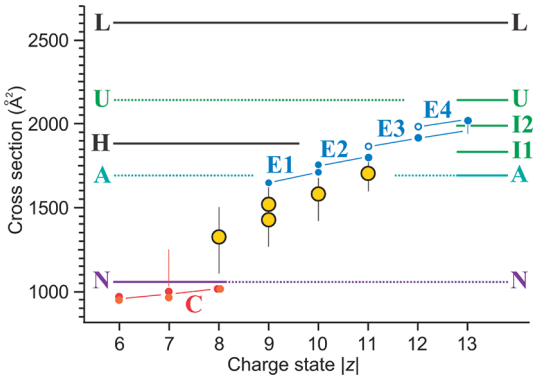

Figure 5. Ubiquitin cross section as a function of charge state $|z|$. Values obtained for sharp peaks in the ion mobility spectrum are shown as small dots (major peaks) or small circles (minor peaks). Weak shoulders on one side of the peak are indicated with a vertical bar spanning the width of the shoulder. Cross sections corresponding to the center of a broad IMS peak are shown as large yellow dots with a vertical bar indicating the width of the peak. There is a family of compact structures **C** with a cross section near 1000 Å^2 (red data for positive, orange for negative ions) and several families of well-defined extended structures above 1600 Å^2 (blue data). The blue data appear to increase in three steps from $z = 9$ to $z = 13$ indicating the presence of four distinct elongated families of structures **E1**−**E4**. The cross section of the native state ($z = 6$−8) is calculated (EHSS) to be ∼1060 Å^2 (solid purple line) and that of the *A* state ($z = 13$) to be 1690 Å^2 (turquoise). Also shown are cross section data for theoretical structures obtained for a helical (**H**) and a linear (**L**) conformation (Figure 1) and for MD structures (metastable intermediates **I1** and **I2** and final unfolded state **U**) of $[M + 13H]^{+13}$ in a solvent-free environment (green).[52] The **U**, **A**, and **N** values are extended with dotted lines over the entire *z*-range for better comparison of the data.

ions ($z = 6$, 7, and 8). The charge state ±6 and ±7 spectra are dominated by one strong peak in the 1000 Å^2 range with the negative ion cross section slightly smaller (by 2−3%) than for positive ions. The spectra of charge states +8 and −8 indicate a strong similarity for the sharp peak at 1000 Å^2 (when present) with respect to position and width but significant differences in the 1100−1500 Å^2 range.

Figure 5 summarizes the ion mobility peak positions as a function of charge state. The position of strong narrow peaks is indicated by a small dot and that of weaker narrow peaks by a small circle. The maximum of a broad feature is shown as a large circle with the width of the peak indicated by a bar. Similarly, shoulders to one side of a peak are marked with a bar. Hence, the spectrum shown in Figure 4b for $z = +7$ is represented by a small red dot at 1000 Å^2 and a bar extending to 1250 Å^2. It can be seen that the position of the sharp peak around 1000 Å^2 is nearly independent of z in the $|z| = 6$−8 range, although a slight increase in cross section with increasing $|z|$ appears to be present. The position of the sharp feature(s) observed for the higher charge states, on the other hand, depends very clearly on z with values increasing from 1650 to 2000 Å^2 over the range from $z = 9$ to 13. Similarly, the broad peaks around 1500 Å^2 also shift to larger cross sections with increasing charge.

To put the experimental cross sections in perspective, a comparison with the size of known ubiquitin structures is useful. The native structure **N** shown in Figure 1 has a corresponding collision cross section in helium of 1150 Å^2 (1D3Z,[38] geometry #1). However, this structure does not correspond to a minimum on the potential energy surface after removal of solvent. A vacuum geometry optimization to the next local minimum in the AMBER force field[57] yields a 10% reduction in cross section (to 1010 Å^2); however, the secondary and tertiary structure is retained as shown in Figure 1. Hence, the compaction in this $z = 0$ geometry is simply due to annealing of the side chains and the unstructured C-terminal residues once solvent is removed. Addition of 6, 7, or 8 charges to this $z = 0$ structure expands the structure by about 5% (to 1050−1070 Å^2) according to AMBER, again leaving the native secondary and tertiary structure intact.

The other known ubiquitin structure, the *A* state (Figure 1 **A**), yields a cross section of 1690 Å^2 after removal of solvent and annealing, substantially less compact than the native state.[52] The cross section values for **N** (1060 Å^2) and **A** are shown in Figure 5 in purple and turquoise, respectively, for comparison with experiment. Also shown in Figure 5 are cross section values for ubiquitin **I1**, **I2**, and **U** structures previously reported for $[M + 13H]^{+13}$.[52] A hypothetical all-helical conformation **H** (Figure 1) where all dihedral ϕ and ψ angles along the backbone are set to −57° and −47°, respectively, has a cross section of 1880 Å^2, and a linear conformation **L** ($\phi = \psi = 180°$) reaches 2600 Å^2.

DISCUSSION

The native state of ubiquitin is very robust and occurs under a wide range of solution conditions. In particular, it is known to be stable under all solution conditions used here with one exception, the condition typically used for ESI: 1% acetic acid in a 1:1 mixture of water and methanol. Interestingly, the ubiquitin ESI mass spectrum obtained for the acidic water−methanol solution is also the one which distinguishes itself from the other spectra (Figure 2): Only in the presence of both methanol and acid do we observe a charge state distribution peaking at 12; under all other conditions it peaks around 7 or 8. Hence, there is a strong correlation between charge state distribution and solution structure, with low charge states for folded solution structures and high charge states for less compact structures. A change of charge state distribution induced by a change in solution condition has previously been observed for a range of proteins, with some studies dating back to the early days of ESI.[58−62] Early on, it was suggested that this effect is due to a change in protein conformation. Here, in the case of ubiquitin with its solution structure known independent of MS, we can unambiguously conclude that the ESI charge state distribution correlates not only with the denaturing potential of the solution but with the actual protein structure in bulk solution.

On the other hand, there is no correlation between the solution charge state distribution and charge states z detected after ESI. Operating the mass spectrometer in positive ion mode, z is around +7 for desolvated ions emerging from water at both neutral and acidic pH (Figure 2c and d). In solution, however, NMR-based titration studies indicate a significant shift in the charge state distribution from pH 7 to pH 3 (1% acidic acid): solution pK_a values lie between 3.1 and 4.5 for all 12 ubiquitin carboxyl groups.[63] In negative ion mode, z is −7 or −8 for desolvated ions sprayed out of pure water (Figure 2f). Hence, the amount of charge present on the protein after ESI is similar in positive and negative ion mode, and it appears to be given by the bulk solution conformation (which is the same in both modes of operation). However, it has been shown that the correlation between charge state distribution and solution structure does not always hold rigorously in the negative ion mode.[64]

Nevertheless, whereas solution conformation is the major factor determining the ESI charge state distribution (at least in positive ion mode), other parameters including solution charge state and surface tension of the solvent[65] may have an additional minor effect and may account, for instance, for the small differences in the spectra of Figure 2b−d. However, these secondary effects are hard to sort out; a higher solution charge state does not, for example, simply translate into more intensity of higher ESI charge states (Figure 2d vs c).

Ion mobility analysis of the most abundant desolvated ubiquitin species following ESI of solutions accommodating the native solution state $\mathbf{N}_{aq}$ indicates there is essentially one family **C** of solvent-free compact structures across charge states ±6, ±7, and ±8. This is evident by inspection of the ion mobility spectra of the most abundant species detected in the mass spectrometer under these solution conditions, $[M + 7H]^{+7}$, $[M - 7H]^{-7}$, and $[M - 8H]^{-8}$ (see mass spectra in Figure 2c−f), and in the case of water−methanol $[M + 8H]^{+8}$ (Figure 2b), indicating one sharp intense peak at a cross section around 1000 Å^2 in all cases (Figure 4b−d). The width of those sharp ion mobility peaks is about twice the expected instrument resolution in all cases, indicating the presence of at least two (and probably more) very similar structures for each of these charge states which do not interconvert on the experimental time scale.

Under solution conditions favoring the *A* state, on the other hand, the most intense peaks in the mass spectrum (Figure 2a) correspond to $[M + 11H]^{+11}$, $[M + 12H]^{+12}$, and $[M + 13H]^{+13}$. The ion mobility spectra of these species show sharp intense peaks at longer drift time, indicating extended desolvated structures **E** in the 1800−2000 Å^2 range (Figure 3, $z = 11-13$ spectra). Again, the sharp **E** peaks are slightly broader than expected for a single conformation. Thus, since $\mathbf{N}_{aq}$ and $\mathbf{A}_{aq}$ yield **C** and **E**, respectively, the only factor having an effect on the ubiquitin shape after desolvation is the solution condition the molecule originated from, and qualitatively (or even semiquantitatively), the shape of the solution structure is preserved into the gas phase.

The fact that the **C** family of structures originates from $\mathbf{N}_{aq}$, that all compact structures have nearly identical cross sections (950−1000 Å^2) across charge states $|z| = 6-8$ (for positive and negative ions), and that the **C** family cross section matches that of a suitably relaxed, desolvated native structure **N** (Figure 5) strongly suggests that the **C** structures feature a natively folded backbone. The slightly broadened ATD peak width could be the result of a limited structural diversity of the native solution structure. A certain structural diversity of the solution native state is expected based on the range of structures which are typically given in an NMR structural analysis of a protein.

On the other hand, there is more structural diversity among the extended structures of charge states 9−13. A glance at Figures 3 and 5 indicates, first, that more than one sharp peak is present for charge states 10−12 in the 1700−2000 Å^2 range and, second, that the structures responsible for these peaks can be grouped into four families **E1**−**E4** of extended structures. The family of the most extended conformation, **E4**, is populated in charge state 13 and as a minor component in $z = 12$. It comprises structures with cross sections around 2000 Å^2. Figure 5 indicates the three families **E1**−**E3** of slightly more compact structures are centered around 1890 Å^2 (**E3**), 1770 Å^2 (**E2**), and 1690 Å^2 (**E1**).

Hence, solutions favoring the *A* state yield a family **E1** of *A* state-like desolvated ions (Figure 5) and families **E2**−**E4** of more extended structures. The fact that cross sections diverge more and more from the *A* state value with increasing charge for $z \geq 11$ is in agreement with a recent theoretical study on $[M + 13H]^{+13}$ which indicates that the lifetime of the *A* state of this ion is only about 30 ns in the desolvated state at 300 K.[52] The ion quickly assumes a more elongated structure and loses all of its secondary structure within 2 ms, a short time scale compared to the ion mobility experiment of ≥50 ms. Since Coulomb repulsion drives unfolding of the protein, the lifetime of a desolvated *A* state ubiquitin ion is expected to increase with decreasing charge state. Hence, *A* state-like $[M + 10H]^{+10}$ ions appear to survive the 100 ms ion mobility experiment, whereas $[M + 11H]^{+11}$ and $[M + 12H]^{+12}$ do not and get stuck in intermediate structures on the way to the fully unfolded state populated by $[M + 13H]^{+13}$. Interestingly, the theoretical work on $[M + 13H]^{+13}$ indicates three distinct steps in the unfolding process: Starting with the initial structure **A**, followed by two intermediates **I1** and **I2**, and ending in the final unfolded state **U**, there are four distinct types of stable (or metastable) structures with cross sections of 1690, 1830, 1990, and 2140 Å^2. Hence, theory may help us understand the nature of the four *A* state-based families of structures observed here, **E1**−**E4**: Whereas the majority of $[M + 10H]^{+10}$ ions are *A* state-like (**E1**), the majority of $[M + 11H]^{+11}$ (**E2**) and $[M + 12H]^{+12}$ ions (**E3**) may be representatives of the two types of intermediates (**I1** and **I2**) on the path to the extended $[M + 13H]^{+13}$ **U** structure (**E4**). In this scheme, all of the higher charge state conformations ($z > 10$) are products of the *A* state: **E1** → **E2** → **E3** → **E4** with **E1** = **A**.

Even though an all-helical conformation **H** has a cross section in general agreement with the intermediate **E2** and **E3** structures between **A** and **U** (Figure 5), theory indicates that the C-terminal helix is the secondary structure element of **A** that is lost first, in the **A** → **I1** transition.[52] The **I1** → **I2** step involves loss of the β-sheet and **I2** → **U** loss of the helix involving residues 24−35 (Figure 1).

Is the extended **U** structure the final annealed gas-phase geometry ultimately populated by all ubiquitin ions? Or is refolding occurring in the gas phase into a low-energy solvent-free conformation, in particular for lower charge states? Annealing experiments carried out in the Clemmer laboratory indicate that the **E4** family of structures comprises the final gas-phase structures for $z = 13$.[33] For $z = 12$ ions, however, **E4** may be an intermediate to slightly more folded **E3′** structures comparable in size to **E3**. Hence, the sequence of conformational changes following ESI may be **E1** → **E2** → **E3** → **E4** → **E3′** for $[M + 12H]^{+12}$ or perhaps simply **E1** → **E2** → **E4** → **E3**. A similar sequence of unfolding and minor refolding is consistent with the annealing data[33] obtained for $[M + 11H]^{+11}$. This raises the question whether gas-phase refolding may be more extensive for lower charge states, for instance $z = 7$.

$[M + 7H]^{+7}$ ions are found to be compact even under solution conditions favoring $\mathbf{A}_{aq}$ (Figure 4b). Is this—admittedly—small population (Figure 2a) of compact $z = 7$ ions the result of a gas-phase collapse of extended *A* state-like $[M + 7H]^{+7}$ ions? IMS work by Clemmer and co-workers indicates this is not the case: Both gas-phase annealing[34] and structural time evolution studies[32] yield extended structures as the final gas-phase product. Hence, observation of compact desolvated $[M + 7H]^{+7}$ ions are not expected to be the result of a gas-phase compaction process **A** → **C** because there is no driving force for compaction. Therefore, the small amount of compact $[M + 7H]^{+7}$ ions detected under *A* state-favoring conditions must originate from the native state ($\mathbf{N}_{aq}$ → **C**) which apparently coexists (as a minor component) with the *A* state in solution under the conditions used to obtain the

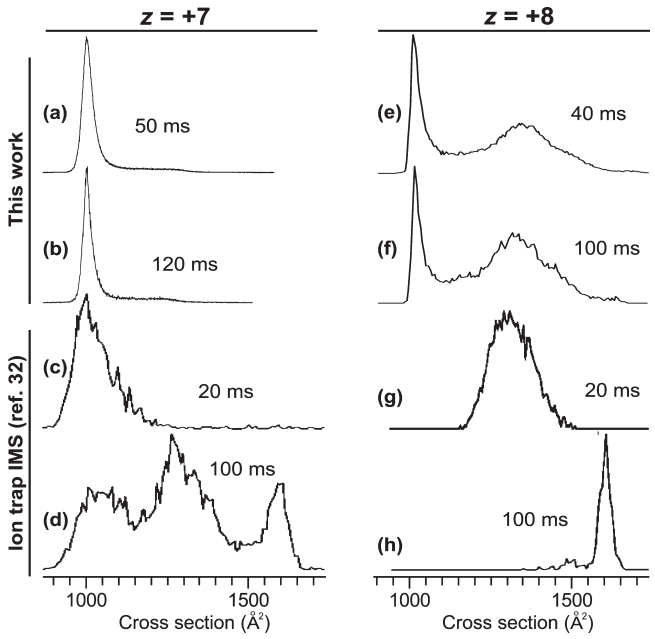

Figure 6. Ion mobility spectra of ubiquitin $[M + zH]^{+z}$ ions obtained in our lab as a function of drift voltage in comparison with ion trap−IMS data reported in the literature.[32] The drift voltages for our $z = 7$ data are (a) 3.9 and (b) 1.5 kV corresponding to a drift time of the major ion species of 50 and 120 ms, respectively. For the published $z = 7$ spectra, ion trap storage times are (c) 20 and (d) 100 ms followed by a ~4 ms IMS analysis. Our $z = 8$ data are shown in (e) for 3.9 and (f) for 1.5 kV drift voltage yielding a 40 and 100 ms drift time, respectively. The published $z = 8$ data are shown in (g) for 20 and (h) 100 ms trap storage time.

spectrum shown in Figure 2a. A comparison of the ATDs in Figure 3b indicates absolutely identical spectra for native state and *A* state-favoring solutions, thereby supporting the presence of native-like $[M + 7H]^{+7}$ structures for all solution conditions. Hence, **A** → **C** folding is not observed following solvent evaporation (at least not below 1300 Å^2, see below), whereas a reaction in the reverse direction, unfolding of **N**, may occur for ubiquitin $z = 7$ ions (given enough time or at elevated temperatures).

Our experiments indicate that unfolding (or any change of structure) of the $[M + 7H]^{+7}$ native state does not occur within 100 ms after ESI under thermal (300 K) conditions. Figure 6a and b shows identical mobility spectra at high (3.9 kV, 50 ms drift time) and low drift field (1.5 kV, 120 ms drift time) and complete absence of any species above 1400 Å^2. Much more rapid decay of the initial $[M + 7H]^{+7}$ structure has previously been reported, likely due to RF-induced collisional heating in the storage ion trap (Figure 6c and d).[32] In those experiments, ESI-generated ions are stored in a quadrupole ion trap for a variable amount of time and subsequently analyzed by IMS. **C** structures are observed to be stable for the first 20 ms of storage in the trap and then to rapidly unfold. The time evolution of the IMS data is complex, but it is rationalized that **C** unfolds partially to structures in the 1300 Å^2 range before unfolding to 1600 Å^2. On the basis of data available from gas-phase H/D-exchange experiments[36] carried out in a Fourier transform ion cyclotron resonance (FTICR) cell containing D_2O vapor, it is further concluded[32] that the distribution of $[M + 7H]^{+7}$ gas-phase structures reaches 70% of extended (1600 Å^2) and 30% of partially folded structures (1300 Å^2) within one hour after ESI. The fact that a bimodal H/D exchange pattern persists for one hour in the FTICR experiment[36] suggests that a gas-phase equilibrium is still not reached after one hour.

The close agreement of the annealed gas-phase $[M + 7H]^{+7}$ cross section (1600 Å^2) with that of the *A* state (1690 Å^2) raises the question whether an **N** → **A** transition following solvent evaporation makes sense. A comparison of the **N** and **A** backbone folding (Figure 1) indicates that there is close agreement for the N-terminal 35 residues. In the native state, however, the N- and C-terminal domains are held together by a β-strand between residues on both ends of the polymer chain, residues 2−6 and 66−71. Loss of this interaction and a concurrent or subsequent $\beta \rightarrow \alpha$ transition in the C-terminal half of the molecule leads straight to the less tightly folded *A* state conformation. Hence, a gas-phase **N** → **A** unfolding step is potentially possible.

Since the **N** → **A** transition appears to provide a plausible unfolding mechanism and since it involves loss of several secondary structure elements, the broad features observed in the ion mobility spectra of charge states 8−10 may well be due to the various intermediates along the **N** → **A** transition. The temporal evolution of ESI-generated $[M + 8H]^{+8}$ conformations presented in the literature[32] indicates unfolding into a 1600 Å^2 conformation is 90% complete within 50 ms. Again, the millisecond time scale for conformational changes is not in agreement with our observations. Under native solution conditions, we observe a significantly populated native-like $[M + 8H]^{+8}$ gas-phase conformation for up to 100 ms drift time with hardly any population of conformations around 1600 Å^2. However, the intensity of the broad IMS feature around 1300 Å^2 is gaining slightly in intensity from 40 to 100 ms (Figure 6e and f). Hence, unfolding appears to occur in our thermal experiment as well but not all the way to the 1600 Å^2 structure and on a time scale well exceeding 100 ms. For $[M - 8H]^{-8}$ anions, there is no change at all in the relative intensities of IMS peaks from 40 (Figure 4c) to 100 ms drift time (data not shown).

These findings indicate clearly that gentle, near-thermal conditions avoiding any high-energy collisions are essential in preserving the solution structure of a protein in the gas phase. Maintaining solution structure may require nonstandard tuning in some mass spectrometers and may not be possible at all in others. It also is not readily compatible with certain MS methods which employ high-energy collisions, such as collision-induced dissociation (CID), or long time scales, such as FTICR and gas-phase H/D-exchange. A recent radical directed dissociation (RDD) study on (3-iodo-tyrosine[59])-ubiquitin may indicate such an incompatibility.[51] In that study, ESI-generated $[M + zH]^{+z}$ ions ($z = 4-10$) are stored in a linear ion trap, irradiated with a laser pulse to knock off the iodine atom, and subsequently fragmented by CID. Ion storage times are of the order of milliseconds (≤30 ms). The radical directed fragmentation patterns indicate little interaction between Tyr[59] and sequence-remote residues for $z = 8-10$ in agreement with at least partially unfolded gas-phase structures. For $z = 6-7$, the natively unstructured C-terminus (specifically Arg[72] and Arg[74]) appears to interact with Tyr[59] in the gas phase. This interaction may be possible without significant disruption of the native conformation, but the authors of the RDD study suggest a nonnative $[M + 6H]^{+6}$ gas-phase structure to explain their data. Part of their reasoning is based on the interpretation of their $z = 4-5$ data which show extensive sequence-remote interactions with Tyr[59] that cannot be explained on the basis of the native state. However, those low +4 and +5 charge states are not observed under native solution conditions (see Figure 2).[59,60] The magnitude of the

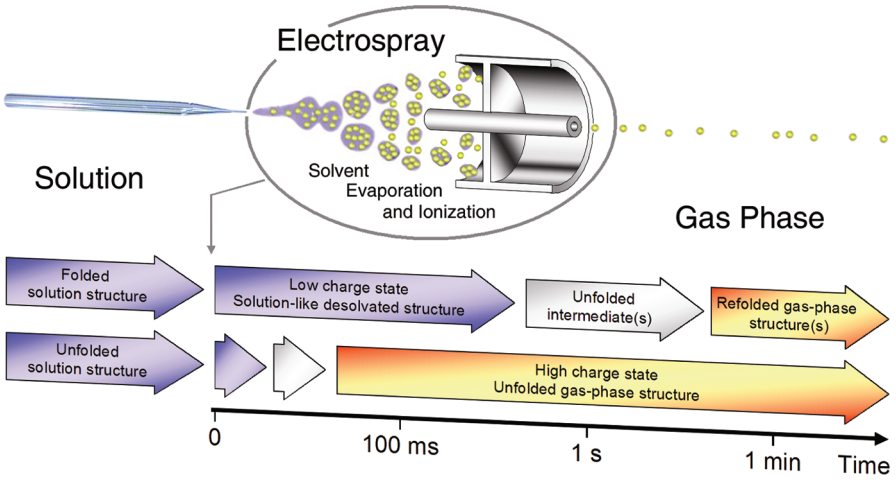

Figure 7. Schematic representation of the conformational changes of a protein in the transition from solution to the gas phase employing an electrospray interface. The protein solution is sprayed from a glass spray tip in the presence of a strong electric field; the solvent evaporates rapidly; and a beam of desolvated protein ions emerging from a capillary can be analyzed by IMS−MS or other methods. A solution of folded protein molecules yields desolvated protein ions in a low charge state which are trapped in a solution-like conformation. The ubiquitin $z = 7$ native state survives more than 100 ms in a solvent-free environment. Unfolding of this ion to one or several intermediates and equilibration into a refolded gas-phase structure takes seconds to minutes. Proteins which are partially or fully unfolded in solution yield medium or high charge states. A ubiquitin *A*-state solution yields $z = 11-13$ ions which unfold after desolvation within 100 ms and subsequently equilibrate into gas-phase structures. High charge states such as ubiquitin $z = 13$ stay unfolded due to Coulomb repulsion.

$z = 4$ and 5 populations is not indicated in the RDD study, but significant $[M + 4H]^{+4}$ and $[M + 5H]^{+5}$ intensities[22,31,66,67] may result from a gas-phase reaction, possibly the dissociation of a dimer (e.g., $[2M + 11H]^{+11} \rightarrow [M + 4H]^{+4} + [M + 7H]^{+7}$).[33,67] This reaction is not expected to result in native monomer conformations. Additional evidence for the absence of solution-like conformations presented in the RDD study is the correlation between extent of sequence-remote RDD and cross sections of extended nonnative structures in the 1600−1700 Å^2 range for $z = 6-10$. The rapid loss of solution structure for these charge states is likely due to harsh (above thermal) gas-phase conditions in the RDD experiment, possibly during ion storage in the ion trap and/or during CID.

MS experiments employing very long time scales may not be in a position to sample solution-like protein structures even if they are carried out under thermal conditions. Such studies include the extensive ECD-FTICR work by Breuker and coworkers on a range of proteins including ubiquitin.[7,44] In these experiments, one ESI-generated charge state is mass selected, equilibrated for several seconds, and exposed to low-energy electrons and its fragment ions subsequently analyzed by FTICR. They use these data to imply sequence-remote hydrogen bonding to specific residues along the backbone and from these data infer structural information. Whereas this type of analysis indicates solution-like structures stable up to 4 s in certain favorable cases,[29] nonnative helical gas-phase structures are inferred for ubiquitin, an extended helix for high charge states and helix bundles with two and three bends for lower charge states.[7,44] However, MD and IMS work by us and others indicates that the equilibrated gas-phase structures of high charge states are somewhat more extended than an α-helix (Figure 5) and those of low charge states more extended (*A* state-like) than a helix bundle.[32,34,52] Nevertheless, whether $[M + 7H]^{+7}$ is a helix bundle or folded otherwise following evaporation of solvent, it can be unfolded by pulsed IR laser excitation, and refolding can be monitored by ECD as a function of time. These data indicate that refolding into the identical starting structure occurs within seconds after laser irradiation,[44] a long time scale compared to a typical high-resolution IMS experiment.

CONCLUSIONS

Our data on ubiquitin support preservation of solution-like structures into the gas phase during the ESI process. The amount of charge picked up by ESI is determined by the degree of folding in bulk solution, and there is no or little correlation to the charge state present in solution. For tightly folded conformations, minor structural adjustments occur during desolvation, evident in slightly different cross sections measured for positive and negative ions. These adjustments are expected to be minimal if the solution and gas-phase charge states happen to be equal or very similar. The native state of ubiquitin $[M + 7H]^{+7}$ ions survives under thermal (300 K) conditions for more than 100 ms after solvent removal without any indication of decay (Figure 6b). The ion mobility spectrum of $[M + 7H]^{+7}$ shows essentially one intense peak with a width corresponding to about twice the instrument resolution indicating a family of slightly different native-like structures. The time required to achieve an equilibrated population of gas-phase $[M + 7H]^{+7}$ structures (at 300 K) appears to exceed several minutes, perhaps hours.[32,36] The transition from a solution-like to an optimum gas-phase structure proceeds via an initial unfolding step.[32] For high charge states ($z = 13$), rapid unfolding (<10 ms) leads directly to the final unfolded gas-phase structure (Figure 5).[52] For low charge states, slow unfolding (>100 ms) leads to one or several metastable intermediates which may further unfold or refold in some cases (most evident for cytochrome c, $z = 9$)[68] into the final gas-phase structure or mixture of structures.[32] These steps of conformational changes following desolvation in the ESI process and their time scales are pictorially summarized in Figure 7.

Do the results presented here for ubiquitin hold for other proteins? Limited data in the literature suggest they do.[11,19−34]

However, great care must be taken to avoid either energizing the ions during the desolvation, sampling, and detection processes or excessively charging the ions leading to Coulomb repulsion-induced unfolding. Hence, IMS−MS when carefully done is an important new tool in structural biochemistry. This is particularly so in aggregating systems where traditional solution structural tools are ineffective.[1,19−21,69,70]

■ ASSOCIATED CONTENT

Supporting Information. Tables of experimental and theoretical cross sections. This material is available free of charge via the Internet at http://pubs.acs.org.

■ AUTHOR INFORMATION

Corresponding Author
*E-mail: bowers@chem.ucsb.edu.

■ ACKNOWLEDGMENT

We are grateful for the support of the National Science Foundation under grant CHE-0909743.

■ REFERENCES

(1) Bleiholder, C.; Dupuis, N. F.; Wyttenbach, T.; Bowers, M. T. *Nat. Chem.* **2011**, *3*, 172–177.
(2) Polfer, N. C.; Oomens, J. *Phys. Chem. Chem. Phys.* **2007**, *9*, 3804–3817.
(3) Wyttenbach, T.; Bowers, M. T. *Top. Curr. Chem.* **2003**, *225*, 207–232.
(4) Clemmer, D. E.; Jarrold, M. F. *J. Mass Spectrom.* **1997**, *32*, 577–592.
(5) Gucinski, A. C.; Somogyi, A.; Chamot-Rooke, J.; Wysocki, V. H. *J. Am. Soc. Mass Spectrom.* **2010**, *21*, 1329–1338.
(6) Stephenson, J. L.; Schaaff, T. G.; McLuckey, S. A. *J. Am. Soc. Mass Spectrom.* **1999**, *10*, 552–556.
(7) Oh, H.; Breuker, K.; Sze, S. K.; Ge, Y.; Carpenter, B. K.; McLafferty, F. W. *Proc. Natl. Acad. Sci. U.S.A.* **2002**, *99*, 15863–15868.
(8) Schnier, P. D.; Price, W. D.; Jockusch, R. A.; Williams, E. R. *J. Am. Chem. Soc.* **1996**, *118*, 7178–7189.
(9) Fenn, J. B. *Angew. Chem., Int. Ed.* **2003**, *42*, 3871–3894.
(10) Uetrecht, C.; Barbu, I. M.; Shoemaker, G. K.; van Duijn, E.; Heck, A. J. R. *Nat. Chem.* **2011**, *3*, 126–132.
(11) Ruotolo, B. T.; Robinson, C. V. *Curr. Opin. Chem. Biol.* **2006**, *10*, 402–408.
(12) Iribarne, J. V.; Thomson, B. A. *J. Chem. Phys.* **1976**, *64*, 2287–2294.
(13) Dole, M.; Mack, L. L.; Hines, R. L. *J. Chem. Phys.* **1968**, *49*, 2240–&.
(14) Kebarle, P.; Tang, L. *Anal. Chem.* **1993**, *65*, A972–A986.
(15) Smith, J. N.; Flagan, R. C.; Beauchamp, J. L. *J. Phys. Chem. A* **2002**, *106*, 9957–9967.
(16) Touboul, D.; Jecklin, M. C.; Zenobi, R. *Rapid Commun. Mass Spectrom.* **2008**, *22*, 1062–1068.
(17) Bruins, A. P. *J. Chromatogr. A* **1998**, *794*, 345–357.
(18) Breuker, K.; McLafferty, F. W. *Proc. Natl. Acad. Sci. U.S.A.* **2008**, *105*, 18145–18152.
(19) Bernstein, S. L.; Wyttenbach, T.; Baumketner, A.; Shea, J. E.; Bitan, G.; Teplow, D. B.; Bowers, M. T. *J. Am. Chem. Soc.* **2005**, *127*, 2075–2084.
(20) Bernstein, S. L.; Dupuis, N. F.; Lazo, N. D.; Wyttenbach, T.; Condron, M. M.; Bitan, G.; Teplow, D. B.; Shea, J. E.; Ruotolo, B. T.; Robinson, C. V.; Bowers, M. T. *Nat. Chem.* **2009**, *1*, 326–331.
(21) Grabenauer, M.; Wyttenbach, T.; Sanghera, N.; Slade, S. E.; Pinheiro, T. J. T.; Scrivens, J. H.; Bowers, M. T. *J. Am. Chem. Soc.* **2010**, *132*, 8816–8818.
(22) Shelimov, K. B.; Clemmer, D. E.; Hudgins, R. R.; Jarrold, M. F. *J. Am. Chem. Soc.* **1997**, *119*, 2240–2248.
(23) Gidden, J.; Ferzoco, A.; Baker, E. S.; Bowers, M. T. *J. Am. Chem. Soc.* **2004**, *126*, 15132–15140.
(24) Baker, E. S.; Bernstein, S. L.; Gabelica, V.; De Pauw, E.; Bowers, M. T. *Int. J. Mass Spectrom.* **2006**, *253*, 225–237.
(25) Baker, E. S.; Bowers, M. T. *J. Am. Soc. Mass Spectrom.* **2007**, *18*, 1188–1195.
(26) Baker, E. S.; Dupuis, N. F.; Bowers, M. T. *J. Phys. Chem. B* **2009**, *113*, 1722–1727.
(27) Wyttenbach, T.; Grabenauer, M.; Thalassinos, K.; Scrivens, J. H.; Bowers, M. T. *J. Phys. Chem. B* **2010**, *114*, 437–447.
(28) Koeniger, S. L.; Merenbloom, S. I.; Clemmer, D. E. *J. Phys. Chem. B* **2006**, *110*, 7017–7021.
(29) Breuker, K.; Brüschweiler, S.; Tollinger, M. *Angew. Chem., Int. Ed.* **2011**, *50*, 873–877.
(30) Liu, L.; Bagal, D.; Kitova, E. N.; Schnier, P. D.; Klassen, J. S. *J. Am. Chem. Soc.* **2009**, *131*, 15980–15981.
(31) Valentine, S. J.; Counterman, A. E.; Clemmer, D. E. *J. Am. Soc. Mass Spectrom.* **1997**, *8*, 954–961.
(32) Myung, S.; Badman, E. R.; Lee, Y. J.; Clemmer, D. E. *J. Phys. Chem. A* **2002**, *106*, 9976–9982.
(33) Koeniger, S. L.; Clemmer, D. E. *J. Am. Soc. Mass Spectrom.* **2007**, *18*, 322–331.
(34) Koeniger, S. L.; Merenbloom, S. I.; Sevugarajan, S.; Clemmer, D. E. *J. Am. Chem. Soc.* **2006**, *128*, 11713–11719.
(35) Baumketner, A.; Bernstein, S. L.; Wyttenbach, T.; Bitan, G.; Teplow, D. B.; Bowers, M. T.; Shea, J. E. *Protein Sci.* **2006**, *15*, 420–428.
(36) Freitas, M. A.; Hendrickson, C. L.; Emmett, M. R.; Marshall, A. G. *Int. J. Mass Spectrom.* **1999**, *187*, 565–575.
(37) Vijay-Kumar, S.; Bugg, C. E.; Cook, W. J. *J. Mol. Biol.* **1987**, *194*, 531–544.
(38) Cornilescu, G.; Marquardt, J. L.; Ottiger, M.; Bax, A. *J. Am. Chem. Soc.* **1998**, *120*, 6836–6837.
(39) Weber, P. L.; Brown, S. C.; Mueller, L. *Biochemistry* **1987**, *26*, 7282–7290.
(40) Di Stefano, D. L.; Wand, A. J. *Biochemistry* **1987**, *26*, 7272–7281.
(41) Stockman, B. J.; Euvrard, A.; Scahill, T. A. *J. Biomol. NMR* **1993**, *3*, 285–296.
(42) Brutscher, B.; Bruschweiler, R.; Ernst, R. R. *Biochemistry* **1997**, *36*, 13043–13053.
(43) Wilkinson, K. D.; Mayer, A. N. *Arch. Biochem. Biophys.* **1986**, *250*, 390–399.
(44) Breuker, K.; Oh, H. B.; Horn, D. M.; Cerda, B. A.; McLafferty, F. W. *J. Am. Chem. Soc.* **2002**, *124*, 6407–6420.
(45) Geller, O.; Lifshitz, C. *J. Phys. Chem. A* **2005**, *109*, 2217–2222.
(46) Robinson, E. W.; Williams, E. R. *J. Am. Soc. Mass Spectrom.* **2005**, *16*, 1427–1437.
(47) Robinson, E. W.; Leib, R. D.; Williams, E. R. *J. Am. Soc. Mass Spectrom.* **2006**, *17*, 1469–1479.
(48) Shvartsburg, A. A.; Li, F.; Tang, K.; Smith, R. D. *Anal. Chem.* **2006**, *78*, 8575–8575.
(49) Purves, R. W.; Barnett, D. A.; Ells, B.; Guevremont, R. *J. Am. Soc. Mass Spectrom.* **2000**, *11*, 738–745.
(50) Purves, R. W.; Barnett, D. A.; Ells, B.; Guevremont, R. *J. Am. Soc. Mass Spectrom.* **2001**, *12*, 894–901.
(51) Ly, T.; Julian, R. R. *J. Am. Chem. Soc.* **2010**, *132*, 8602–8609.
(52) Segev, E.; Wyttenbach, T.; Bowers, M. T.; Gerber, R. B. *Phys. Chem. Chem. Phys.* **2008**, *10*, 3077–3082.
(53) Hernandez, H.; Robinson, C. V. *Nat. Protoc.* **2007**, *2*, 715–726.
(54) Kemper, P. R.; Dupuis, N. F.; Bowers, M. T. *Int. J. Mass Spectrom.* **2009**, *287*, 46–57.
(55) Mason, E. A.; McDaniel, E. W. *Transport properties of ions in gases*; Wiley: New York, 1988.
(56) Shvartsburg, A. A.; Jarrold, M. F. *Chem. Phys. Lett.* **1996**, *261*, 86–91.

(57) Case, D. A., et al. *Amber 8*; University of California: San Francisco, 2004.
(58) Chowdhury, S. K.; Katta, V.; Chait, B. T. *J. Am. Chem. Soc.* **1990**, *112*, 9012–9013.
(59) Katta, V.; Chait, B. T. *Rapid Commun. Mass Spectrom.* **1991**, *5*, 214–217.
(60) Wilson, D. J.; Konermann, L. *Anal. Chem.* **2003**, *75*, 6408–6414.
(61) Yan, X. G.; Watson, J.; Ho, P. S.; Deinzer, M. L. *Mol. Cell. Proteomics* **2004**, *3*, 10–23.
(62) Konermann, L. *J. Phys. Chem. B* **2007**, *111*, 6534–6543.
(63) Sundd, M.; Iverson, N.; Ibarra-Molero, B.; Sanchez-Ruiz, J. M.; Robertson, A. D. *Biochemistry* **2002**, *41*, 7586–7596.
(64) Konermann, L.; Douglas, D. J. *J. Am. Soc. Mass Spectrom.* **1998**, *9*, 1248–1254.
(65) Iavarone, A. T.; Williams, E. R. *J. Am. Chem. Soc.* **2003**, *125*, 2319–2327.
(66) Zhao, Q.; Soyk, M. W.; Schieffer, G. M.; Fuhrer, K.; Gonin, M. M.; Houk, R. S.; Badman, E. R. *J. Am. Soc. Mass Spectrom.* **2009**, *20*, 1549–1561.
(67) Jurchen, J. C.; Williams, E. R. *J. Am. Chem. Soc.* **2003**, *125*, 2817–2826.
(68) Badman, E. R.; Myung, S.; Clemmer, D. E. *J. Am. Soc. Mass Spectrom.* **2005**, *16*, 1493–1497.
(69) Dupuis, N. F.; Wu, C.; Shea, J. E.; Bowers, M. T. *J. Am. Chem. Soc.* **2009**, *131*, 18283–18292.
(70) Dupuis, N. F.; Wu, C.; Shea, J. E.; Bowers, M. T. *J. Am. Chem. Soc.* **2011**, *133*, 7240–7243.